SUPPLEMENTARY INFORMATION

doi:10.1038/nature10461

Supplementary Information for "Laser cooling of a nanomechanical oscillator into its quantum ground state"

Jasper Chan,[1] T. P. Mayer Alegre,[1,†] Amir H. Safavi-Naeini,[1] Jeff T. Hill,[1] Alex Krause,[1] Simon Gröblacher,[1,2] Markus Aspelmeyer,[2] and Oskar Painter[1,*]

[1] *Thomas J. Watson, Sr., Laboratory of Applied Physics, California Institute of Technology, Pasadena, CA 91125*

[2] *Vienna Center for Quantum Science and Technology (VCQ), Faculty of Physics, University of Vienna, Boltzmanngasse 5, A-1090 Vienna, Austria*

(Dated: August 11, 2011)

DERIVATION OF TRANSDUCED SIGNAL

We begin by modeling the optomechanical system with the Hamiltonian

$$\hat{H} = \hbar\Delta\hat{a}^\dagger\hat{a} + \hbar\omega_m\hat{b}^\dagger\hat{b} + \hbar g(\hat{b}^\dagger + \hat{b})\hat{a}^\dagger\hat{a} + i\hbar\sqrt{\frac{\kappa_e}{2}}\alpha_{\mathrm{in},0}(\hat{a} - \hat{a}^\dagger), \tag{S1}$$

where $\Delta = \omega_o - \omega_\mathrm{l}$, with laser frequency ω_l, optical mode frequency ω_o and mechanical mode frequency ω_m. Here $\hat{a}$ ($\hat{a}^\dagger$) and $\hat{b}$ ($\hat{b}^\dagger$) are respectively the annihilation (creation) operators of photon and phonon resonator quanta, g is the optomechanical coupling rate corresponding physically to the shift in the optical mode frequency due to the zero-point fluctuations ($x_\mathrm{zpf} = \sqrt{\hbar/2m\omega_m}$, m motional mass) of the phonon mode.

Classical Derivation of Observed Spectra

By making the substitutions

$$\hat{a} \to \alpha = \sum_q \alpha_q e^{-iq\omega_m t}, \quad \hat{b} \to \beta_0 e^{-i\omega_m t}, \tag{S2}$$

we can treat the system classically by representing the photon amplitudes as a Fourier decomposition of sidebands. Notice that the infinite summation over each sideband order q, can be relaxed to a few orders in the sideband resolved regime ($\kappa \ll \omega_m$). The phonon amplitude, β_0, is the classical mechanical excitation amplitude. For an oscillator undergoing thermal Brownian motion, β_0, is a stochastic process. We assert the stochastic nature of the variable, at the end of the derivation where the power spectral density is calculated. The equation of motion for the slowly varying component is then

$$-i\omega_m \sum_q q\alpha_q e^{-iq\omega_m t} = -\left(i\Delta + \frac{\kappa}{2}\right)\sum_q \alpha_q e^{-iq\omega_m t} - ig\beta_0 \sum_q \alpha_q \left(e^{-i(q+1)\omega_m t} + e^{-i(q-1)\omega_m t}\right) - \sqrt{\frac{\kappa_e}{2}}\alpha_{\mathrm{in},0}, \tag{S3}$$

where we introduce the cavity (optical) energy loss rate, κ, and the cavity coupling rate, κ_e. This can be written as a system of equations $\mathbf{M}\cdot\vec{\alpha} = \mathbf{a_{in}}$ where

$$M_{pq} = \left(i(\Delta - p\omega_m) + \frac{\kappa}{2}\right)\delta_{pq} + ig\beta_0(\delta_{p,q+1} + \delta_{p,q-1}), \tag{S4}$$

$$\mathrm{a}_{\mathrm{in},p} = -\sqrt{\frac{\kappa_e}{2}}\alpha_{\mathrm{in},0}\delta_{p0}. \tag{S5}$$

By truncating and inverting the coupling matrix $\mathbf{M}$ one can determine each one of the sidebands amplitude as $\alpha_q = (M^{-1})_{qp}\ \mathrm{a}_{\mathrm{in},p}$ and therefore determine the steady state power leaving the cavity to be

$$\alpha_\mathrm{out} = \alpha_{\mathrm{in},0} + \sqrt{\frac{\kappa_e}{2}}\alpha, \tag{S6}$$

where we assumed that the input pump is not depleted by the cavity, which is the frame of interest of this work. In this case the total power measured at the photodetector will be proportional to

$$|\alpha_{\rm out}|^2 = \left|\alpha_{\rm in,0} + \sqrt{\frac{\kappa_e}{2}}\alpha\right|^2 = |\alpha_{\rm in,0}|^2 + \frac{\kappa_e}{2}\sum_q\sum_p \alpha_q\alpha_p^* e^{-i(q-p)\omega_m t} + 2{\rm Re}\left\{\alpha_{\rm in,0}\sqrt{\frac{\kappa_e}{2}}\sum_q \alpha_q e^{iq\omega_m t}\right\}. \quad \text{(S7)}$$

Simplified Result Under Resolved Sideband Limit ($\omega_m > \kappa/2$)

The equations presented in the previous section are exact and therefore can be solved for any case. However our interests lie in the so-called resolved sideband limit, $\omega_m > \kappa/2$, where further simplification can be done. Specifically for our system, $\omega_m/2\pi = 3.68$ GHz, $\kappa/2\pi = 500$ MHz putting us well within this limiting case.

Additionally, in the cavities studied, the optomechanical phase-modulation factor (proportional to g/ω_m), is much less than 10^{-3}. As such, only the $\omega = \omega_{\rm l} \pm \omega_m$ sidebands ($q = \pm 1$) are significant and $\alpha_0 \gg \alpha_\pm$. Truncating the matrix equations appropriately, we find

$$\alpha_0 = \frac{-\sqrt{\kappa_e/2}\alpha_{\rm in,0}}{i\Delta + \kappa/2}, \quad \text{(S8)}$$

$$\alpha_\pm = \frac{-ig\beta_0\alpha_0}{i(\Delta \mp \omega_m) + \kappa/2}, \quad \text{(S9)}$$

where $\alpha_{\rm in,0} = \sqrt{N_{\rm in}}$, $N_{\rm in} = P_{\rm in}/\hbar\omega_0$ and $P_{\rm in}$ the input power at the cavity. We note that $n_c \equiv |\alpha_0|^2$ is the intracavity photon number.

In the sideband resolved limit, we have $|\alpha_{\rm in,0}| > |\sqrt{\kappa_e/2}\alpha_0| > |\sqrt{\kappa_e/2}\alpha_\pm|$. Therefore the photodetector signal is predominantly composed of the mixing between sidebands with the input pump beam and terms containing $|\alpha_0|^2$, and can be written as [1]

$$\begin{aligned}
|\alpha_{\rm out}|^2 &= |\alpha_{\rm in,0}|^2 + \sqrt{\frac{\kappa_e}{2}}\alpha_{\rm in,0}(\alpha_0 + \alpha_0^*) + \frac{\kappa_e}{2}|\alpha_0|^2 + \ldots \\
&\quad \sqrt{\frac{\kappa_e}{2}}\alpha_{\rm in,0}(\alpha_- e^{-i\omega_m t} + \alpha_-^* e^{i\omega_m t}) + \ldots \\
&\quad \sqrt{\frac{\kappa_e}{2}}\alpha_{\rm in,0}(\alpha_+ e^{i\omega_m t} + \alpha_+^* e^{-i\omega_m t}) + \mathcal{O}(|\alpha_0||\alpha_\pm|) \\
&\approx |\alpha_{\rm in,0}|^2\left|1 - \frac{\kappa_e/2}{i\Delta + \kappa/2}\right|^2 + \ldots \\
&\quad \cos(\omega_m t)\Big[|A_+|\cos(\varphi_+) + |A_-|\cos(\varphi_-)\Big] + \ldots \\
&\quad \sin(\omega_m t)\Big[|A_+|\sin(\varphi_+) - |A_-|\sin(\varphi_-)\Big],
\end{aligned} \quad \text{(S10)}$$

where $A_\pm \equiv 2\sqrt{\kappa_e/2}\ \alpha_{\rm in,0}\alpha_\pm = |A_\pm|\exp(-i\varphi_\pm)$. We can easily recognize the first term in Equation (S10) as the DC cavity transmission spectra. The remaining two terms compose the total power at the mechanical frequency $P_{\rm SB}(\omega_m) = \hbar\omega_0\sqrt{A_{\rm cos}^2 + A_{\rm sin}^2}$, where $A_{\rm cos} = |A_+|\cos(\varphi_+) + |A_-|\cos(\varphi_-)$ and $A_{\rm sin} = |A_+|\sin(\varphi_+) - |A_-|\sin(\varphi_-)$.

Given a mechanical system which is oscillating coherently at a frequency ω_m (β_0 is simply a complex number) the single sided spectral density of the power at the detector, as a function of the laser detuning Δ, and frequency ω, will be given by

$$\begin{aligned}
S_{\rm PP}(\omega,\Delta) &= \hbar^2\omega_0^2\kappa_e^2\left|\alpha_{\rm in,0}\right|^4 \times \left|\frac{ig\beta_0}{(i\Delta + \kappa/2)(i(\Delta - \omega_m) + \kappa/2)}\right|^2 \times \delta(\omega - \omega_m) \quad \text{(S11)} \\
&= \hbar^2\omega_0^2\frac{g^2|\beta_0|^2\kappa_e^2\left|\alpha_{\rm in,0}\right|^4}{(\Delta^2 + (\kappa/2)^2)((\Delta - \omega_m)^2 + (\kappa/2)^2)} \times \delta(\omega - \omega_m).
\end{aligned}$$

For mechanical systems undergoing random oscillations, the important quantity is the power spectral density of the detected signal. Since this is calculated from the autocorrelation functions, it will contain products of the form $\beta_0^*(t)\beta_0(t')$. Classically, these averages may be calculated from the Boltzmann distribution, and can be replaced with $\bar{n}_T = k_B T_b/\hbar\omega_m$, with k_B the Boltzmann constant, and T_b the bath temperature. Additionally, since the measured sideband is blue of the pump frequency ($\omega_l + \omega_m$), from the quantum theory [2, 3], and the derivation below, the proper ordering to be used is the normal one ($b^\dagger b$), and thus the expectation values may be replaced with $\bar{n}$, the number of phonons occupying the mechanical mode. As such, we can effectively use the derivations shown above, in both the classical and quantum cases, substituting β_0 by $\sqrt{\bar{n}}$, and replacing the delta functions $\delta(\omega - \omega_m)$ with unit-area Lorentzian functions. A fully quantum mechanical derivation of this result is shown below.

Quantum Mechanical Derivation of Observed Spectra

In this section we use the following conventions for Fourier transforms and spectral densities. Given an operator A, we take

$$\hat{A}(t) = \frac{1}{\sqrt{2\pi}} \int_{-\infty}^{\infty} d\omega \; e^{-i\omega t} \hat{A}(\omega), \tag{S12}$$

$$\hat{A}(\omega) = \frac{1}{\sqrt{2\pi}} \int_{-\infty}^{\infty} dt \; e^{i\omega t} \hat{A}(t), \tag{S13}$$

$$S_{AA}(\omega) = \int_{-\infty}^{\infty} d\tau \; e^{i\omega\tau} \langle \hat{A}^\dagger(t+\tau)\hat{A}(t)\rangle. \tag{S14}$$

Additionally we define the symmetrized spectral density as $\bar{S}_{AA}(\omega) = \frac{1}{2}(S_{AA}(\omega) + S_{AA}(-\omega))$, and one-sided spectral densities which are those measured by the spectrum analyzer as $\bar{S}_A(\omega) = 2\bar{S}_{AA}(\omega)$. Starting from the quantum-optical Langevin equations for the mechanical ($\hat{b}$) and optical ($\hat{a}$) annihilation operators,

$$\dot{\hat{b}}(t) = -\left(i\omega_m + \frac{\gamma_i}{2}\right)\hat{b} - ig\hat{a}^\dagger\hat{a} - \sqrt{\gamma_i}\hat{b}_{\rm in}, \tag{S15}$$

$$\dot{\hat{a}}(t) = -\left(i\Delta + \frac{\kappa}{2}\right)\hat{a} - ig\hat{a}(\hat{b}^\dagger + \hat{b}) - \sqrt{\kappa_e/2}\hat{a}_{\rm in}(t) - \sqrt{\kappa'}\hat{a}_{{\rm in},i}(t), \tag{S16}$$

we linearize the equations about a large optical field intensity by displacing $\hat{a} \to \alpha_0 + \hat{a}$. Then in Fourier domain the fluctuations are then given by

$$\hat{b}(\omega) = \frac{-\sqrt{\gamma_i}\hat{b}_{\rm in}(\omega)}{i(\omega_m - \omega) + \gamma_i/2} - \frac{iG(\hat{a}(\omega) + \hat{a}^\dagger(\omega))}{i(\omega_m - \omega) + \gamma_i/2}, \tag{S17}$$

$$\hat{a}(\omega) = \frac{-\sqrt{\kappa_e/2}\hat{a}_{\rm in}(\omega) - \sqrt{\kappa'}\hat{a}_{{\rm in},i} - iG(\hat{b}(\omega) + \hat{b}^\dagger(\omega))}{i(\Delta - \omega) + \kappa/2}, \tag{S18}$$

where $\kappa' = \kappa - \kappa_e/2$ denotes all the optical loss channels which go undetected (i.e. information is lost) and $G = g\alpha_0$. For an ideal measurement, $\kappa_e/2 = \kappa$, and $\kappa' = 0$, so the intrinsic vacuum fluctuations ($\hat{a}_{{\rm in},i}$) never enter the optical cavity. For a double sided coupling scheme, such as the one with a fiber taper, $\kappa = \kappa_i + \kappa_e$, and so $\kappa' = \kappa_e/2$ at best, due to the back reflection from the cavity, which contains information about the mechanics which is lost.

We account for all the fluctuations (vacuum and thermal) incident on the photodetector, and calculating the spectra of each term, we find the heterodyne detected signal. Using Equations (S17) and (S18) we arrive at the operator for the mechanical fluctuations,

$$\begin{aligned}\hat{b}(\omega) = &\frac{-\sqrt{\gamma_i}\hat{b}_{\rm in}(\omega)}{i(\omega_m - \omega) + \gamma/2} + \dots \\ &\frac{iG}{i(\Delta - \omega) + \kappa/2}\frac{\sqrt{\kappa_e/2}\hat{a}_{\rm in}(\omega) + \sqrt{\kappa'}\hat{a}_{{\rm in},1}(\omega)}{i(\omega_m - \omega) + \gamma/2} + \dots \\ &\frac{iG}{-i(\Delta + \omega) + \kappa/2}\frac{\sqrt{\kappa_e/2}\hat{a}^\dagger_{\rm in}(\omega) + \sqrt{\kappa'}\hat{a}^\dagger_{{\rm in},i}(\omega)}{i(\omega_m - \omega) + \gamma/2},\end{aligned} \tag{S19}$$

where ω_m is now the optical-spring shifted mechanical frequency, and $\gamma = \gamma_i + \gamma_{\rm OM}$, the optically damped mechanical loss-rate.

Simplified Result Under RWA ($\kappa^2/16\omega_m^2 \ll 1$) and Weak-Coupling ($G \ll \kappa$)

Assuming that $\Delta = \omega_m$ and that we care mainly about the system response around ω_m (where $\hat{b}(\omega)$ is peaked), the relation (S19) can be simplified to

$$\hat{b}(\omega) = \frac{-\sqrt{\gamma_i}\hat{b}_{\rm in}(\omega)}{i(\omega_m-\omega)+\gamma/2} + \frac{2iG}{\kappa}\frac{\sqrt{\kappa_e/2}\hat{a}_{\rm in}+\sqrt{\kappa'}\hat{a}_{{\rm in},i}(\omega)}{i(\omega_m-\omega)+\gamma/2} + \mathcal{O}\left(\frac{G}{2\omega_m}\right) \tag{S20}$$

and we drop the term $\propto \frac{1}{2\omega_m}$ in the rotating wave approximation (RWA).

We find using the input-output boundary condition

$$\begin{aligned}
\hat{a}_{\rm out}(\omega) &= \hat{a}_{\rm in}(\omega) + \sqrt{\kappa_e/2}\hat{a}(\omega) + E_{\rm LO}\delta(\omega) \\
&= \hat{a}_{\rm in}(\omega)\left(1 - \frac{\kappa_e}{\kappa} + \frac{4|G|^2}{\kappa}\frac{\kappa_e}{2\kappa}\frac{1}{i(\omega_m-\omega)+\gamma/2}\right) + \dots \\
&\quad \hat{a}_{{\rm in},i}(\omega)\left(-\sqrt{\frac{2\kappa'\kappa_e}{\kappa^2}} + \frac{4|G|^2}{\kappa}\sqrt{\frac{\kappa'\kappa_e}{2\kappa^2}}\frac{1}{i(\omega_m-\omega)+\gamma/2}\right) + \dots \\
&\quad \hat{b}_{\rm in}(\omega)\left(iG\sqrt{\frac{2\gamma_i\kappa_e}{\kappa^2}}\frac{1}{i(\omega_m-\omega)+\gamma/2}\right) + E_{\rm LO}\delta(\omega) \\
&= s_{11}(\omega)\hat{a}_{\rm in}(\omega) + n_{\rm opt}(\omega)\hat{a}_{{\rm in},i}(\omega) + s_{12}(\omega)\hat{b}_{\rm in}(\omega) + E_{\rm LO}\delta(\omega)
\end{aligned} \tag{S21}$$

with the scattering matrix elements above defined as in [4]. For the case where the mechanical bath is at zero temperature, the spectral density will be given simply by $|s_{11}(\omega)|^2 + |n_{\rm opt}(\omega)|^2 + |s_{12}(\omega)|^2 = 1$, as a result of all input fluctuations being uncorrelated, and therefore no feature is present at the mechanical frequency.

For the case of the $n_b > 0$, we find the autocorrelation of the detected normalized photocurrent $\hat{I}(t) = \hat{a}_{\rm out}(t) + \hat{a}^\dagger_{\rm out}(t)$ to be

$$\begin{aligned}
S_{II}(\omega) &= |s_{11}(\omega)|^2 + |n_{\rm opt}(\omega)|^2 + |s_{12}(\omega)|^2(n_b+1) + |s_{12}(-\omega)|^2 n_b \\
&= 1 + n_b(|s_{12}(\omega)|^2 + |s_{12}(-\omega)|^2) \\
&= 1 + \frac{\kappa_e}{2\kappa}\frac{4|G|^2}{\kappa}\left(\frac{\gamma_i n_b/\gamma}{(\omega_m-\omega)^2+(\gamma/2)^2} + \frac{\gamma_i n_b/\gamma}{(\omega_m+\omega)^2+(\gamma/2)^2}\right) \\
&= 1 + \frac{\kappa_e}{2\kappa}\frac{8|G|^2}{\kappa}\bar{S}_{bb}(\omega),
\end{aligned} \tag{S22}$$

where for the last step we've used the fact that in the highly sideband-resolved regime, $\bar{n} = \gamma_i n_b/\gamma$, and $\bar{S}_{bb}(\omega)$ the symmetrized form of

$$S_{bb}(\omega) = \frac{\gamma\bar{n}}{(\omega_m+\omega)^2+(\gamma/2)^2}. \tag{S23}$$

Optomechanical Damping

For the case where $\Delta = \omega_m$ (pumping on the red side of the cavity), the steady-state phonon amplitude can be written for a sideband resolved system far from strong coupling as [2, 3]

$$\bar{n} = \frac{\gamma_i}{\gamma_{\rm OM}+\gamma_i}n_b, \tag{S24}$$

with n_b the equilibrium mechanical mode occupation number determined by the mechanical bath temperature, γ_i the mechanical coupling rate to the bath and

$$\gamma_{\rm OM} = \frac{4g^2|\alpha_0|^2}{\kappa}, \tag{S25}$$

the resonant optomechanical damping rate.

Effect of Optical Noise on Thermometry

In the measurements of this work, the same optical laser beam used to cool the mechanical oscillator is also used to detect its mechanical motion. Photodetection of the transmitted cooling beam and the scattered light by the mechanical oscillator produce a heterodyne output signal proportional to the mechanical motion. This also means that fluctuations in the cooling laser beam input that are fed into the mechanical system, are also read out by a beam containing the same fluctuations. In addition to potentially raising the phonon number beyond the quantum-back-action limit (in the case of added technical laser noise beyond shot-noise), noise on the input cooling beam can also lead to a coherent cancellation effect at the read-out called "noise squashing" which may cause the mechanical mode occupation to be inferred incorrectly (note that this effect can also be understood in terms of the recently demonstrated electromagnetically induced transparency (EIT), whereby noise photons are transmitted and/or reflected through a transparency window created by the cooling beam). Noise squashing has been studied in low frequency mechanical systems, where excess laser phase noise can be an issue, and in recent microwave work where the electromagnetic cavity is populated with residual photons [5]. In this work we operate in the optical domain where thermal cavity photons are essentially nonexistent and the frequencies of the mechanical oscillators of interest are well beyond that which makes our cooling laser effectively quantum-limited. Nevertheless, in order to rule out additional noise sources (such as thermo-refractive cavity frequency noise [6] or other intracavity nonlinear optical processes), we consider here theoretically and experimentally the effects of noise photons coming from both (i) outside (e.g. laser phase noise) and (ii) inside (e.g. the above-mentioned thermo-refractive cavity noise) the optical cavity. In brief, we show theoretically that the additional cavity noise photons cause an offset in the measured background (broadband) NPSD, which when compared in magnitude to the narrowband Lorentzian signal generated by the mechanical system can be used to assess the impact of the added noise on the inferred phonon population from the measured spectrum. We present the measured offset in the background NPSD versus cooling beam power (in units of intracavity photon number, n_c) for the cooling data of Figure (4b) in the main text, and compare it with the measured narrowband Lorentzian signal level, indicating that any added noise photons produce at most a 4% uncertainty in the inferred phonon occupancy of the mechanical oscillator.

The autocorrelation of the normalized photocurrent found in Equation (S22) was derived with the assumption that all optical noise inputs were in the vacuum state and thus had vacuum correlations. Additional noise may be incorporated by assuming that the optical noise inputs instead have some real photon occupancy. For example, excess optical noise input from the laser due to either phase or intensity noise can have an effective occupancy n_L with correlations in time given by

$$\langle \hat{a}^\dagger_{\rm in}(t)\hat{a}_{\rm in}(t')\rangle = n_L\delta(t-t'), \tag{S26}$$

$$\langle \hat{a}_{\rm in}(t)\hat{a}^\dagger_{\rm in}(t')\rangle = (n_L+1)\delta(t-t'). \tag{S27}$$

In the frequency domain, the input noise operators satisfy the relations

$$\langle \hat{a}^\dagger_{\rm in}(\omega)\hat{a}_{\rm in}(\omega')\rangle = n_L\delta(\omega+\omega'), \tag{S28}$$

$$\langle \hat{a}_{\rm in}(\omega)\hat{a}^\dagger_{\rm in}(\omega')\rangle = (n_L+1)\delta(\omega+\omega'). \tag{S29}$$

The correlation relations for optical noise stemming from intrinsic damping internal to the cavity, $\hat{a}_{{\rm in},i}(t)$, can be defined in an analogous way, with $n_{L,i}$ representing the intrinsic optical noise occupation factor of the cavity (this could correspond to a thermal noise sources of photons, but could also represent other intracavity nonlinear optical processes).

In the resolved sideband limit, and for a cooling laser beam with frequency positioned a mechanical frequency below that of the cavity resonance (the red cavity sideband), it is the excess photonic noise in the upper frequency sidebands that predominantly enter the cavity, drive the mechanical motion, and interfere with the cavity output signal. As such we implicitly consider here only upper sideband excess cooling laser noise, and don't differentiate between intensity and phase noise on the laser. We find that given the correlation functions above, the cooled mechanical oscillator occupation number is modified from that of quantum-limited back-action cooling to,

$$\bar{n} = \frac{\gamma_i}{\gamma_{\rm OM}+\gamma_i}n_b + \frac{\gamma_{\rm OM}}{\gamma_{\rm OM}+\gamma_i}\left(\frac{\kappa_e}{2\kappa}n_L + \frac{\kappa'}{\kappa}n_{L,i}\right). \tag{S30}$$

To calculate the detected signal we generalize Equation (S22),

$$S_{II}(\omega) = |s_{11}(\omega)|^2(n_L+1) + |n_{\rm opt}(\omega)|^2(n_{L,i}+1) + |s_{12}(\omega)|^2(n_b+1) + \ldots$$
$$|s_{11}(-\omega)|^2 n_L + |n_{\rm opt}(-\omega)|^2 n_{L,i} + |s_{12}(-\omega)|^2 n_b,$$

which reduces after some algebraic manipulation to

$$S_{II}(\omega) = 1 + N_{\rm BG} + \frac{\kappa_e}{2\kappa}\frac{8|G|^2}{\kappa}\bar{S}_{bb}^{\rm inf}(\omega), \tag{S31}$$

for frequencies $\omega \approx \omega_m$. Here the optical cavity bandwidth has been implicitly assumed to be much broader than the mechanical bandwidth (hence the constant excess background $N_{\rm BG}$). The (naively) inferred phonon number $\bar{n}^{\rm inf}$ is derived from the area under the positive frequency Lorentzian of the symmetrized $\bar{S}_{bb}^{\rm inf}(\omega)$,

$$\bar{S}_{bb}^{\rm inf}(\omega > 0) = \frac{1}{2}\left(\frac{\gamma\bar{n}^{\rm inf}}{(\omega_m - \omega)^2 + (\gamma/2)^2}\right). \tag{S32}$$

This inferred phonon number $\bar{n}^{\rm inf}$ is not generally equal to the actual mechanical mode occupation $\bar{n}$. For our case of a side-coupled optical cavity in the under-coupled regime (which satisfies $\kappa_e < \kappa$), it can be shown in the high cooperativity limit ($\gamma_{\rm OM} \gg \gamma_i$) that

$$N_{\rm BG} = \left(1 - \frac{\kappa_e}{\kappa}\right)^2 n_L \tag{S33}$$

$$\bar{n}^{\rm inf} = \bar{n} + \left(1 - \frac{\kappa_e}{\kappa}\right) n_L. \tag{S34}$$

Here we've ignored the contribution of $n_{L,i}$ for simplicity (the final conclusions of this section are unaffected). In this case, the inferred phonon number will actually always be *larger* than the true mechanical oscillator phonon occupancy. This is, however, not generally true, but depends upon whether one is measuring in reflection or transmission, or whether the noise is coming from an intracavity source (in the case of an intrinsic cavity photon noise source ($n_{L,i}$) the results are similar, although in both reflection and transmission measurement mode, the inferred phonon number always underestimates the true phonon occupancy).

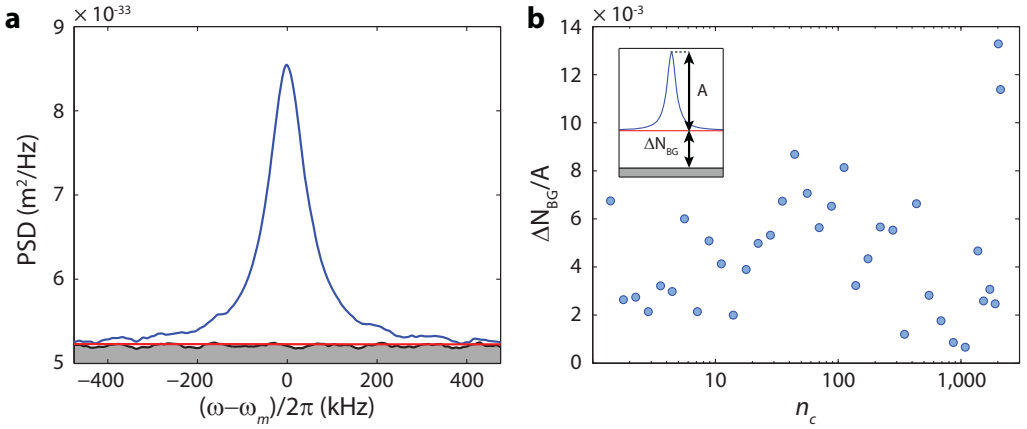

FIG. S1: **Optical noise analysis.** **a**, Typical recorded cooling spectrum showing that the background of the measured Lorentzian (red line) is nearly indistinguishable from the far-detuned background spectrum (black line). **b**, Plot versus cooling beam power of the ratio between the background difference $\Delta N_{\rm BG}$ and the peak of the mechanical mode signal A as defined in the text. Inset shows A and $\Delta N_{\rm BG}$ for a situation in which the background offset is exaggerated.

In order to measure the noise photons present in our experiment we can use the filtering properties of the optical cavity. The details are slightly different between external and internal noise sources, but the overall result is similar. As such, we again just consider the effects of noise on the input cooling beam, n_L. This excess laser noise is determined by making a second measurement of the optical transmission NPSD with the cooling beam far-detuned from the cavity (several mechanical frequencies in practice). In the far-detuned case the NPSD at the mechanical frequency reads $S_{II}(\omega_m) = 1 + n_L$ ($N_{\rm BG,detuned} = n_L$). Comparing to the background level in Equation (S33), the difference around the mechanical frequency in the background of the NPSD taken far-detuned and the background of the spectrum taken during a cooling run (detuning $\Delta = -\omega_m$) may be used to estimate the magnitude of n_L and place bounds on the difference between $\bar{n}$ and the measured $\bar{n}^{\rm inf}$. The amplitude of the narrowband Lorentzian signal peak from Equation (S31), is $A = 4\kappa_e/\kappa\bar{n}^{\rm inf}$. By doing a background subtraction of the far-detuned measured RF spectra from

the cooling spectra, we can fit A and $\Delta N_{\rm BG} = N_{\rm BG} - N_{\rm BG,detuned}$ for each cooling beam power. In this way, any amplifier and shot noise in the output can be subtracted, leaving only a background noise floor proportional to the excess cavity photon noise, which we can then calibrate against the transduced mechanical signal level. In Figure (S1) we show a plot of a typical measured cooling and far-detuned noise spectrum pair for a single cooling beam power along with the deduced ratio $\Delta N_{\rm BG}/A$ for each cooling beam power. Crucially, the ratio $\Delta N_{\rm BG}/A$ is seen to be roughly cooling beam power independent and at a level of less than 1.5%. This observation allows us to rule out any significant noise "squashing" related effects in our measurement as the contribution from background cavity noise photons is on the order of this ratio ($|\Delta N_{\rm BG}/A| \approx n_L/2\bar{n}$ for $n_L/\bar{n} \ll 1$ and $\kappa_e/\kappa \ll 1$). For all cases of interest (noise source external or internal to the cavity, etc.), we find a maximum deviation between $\bar{n}^{\rm inf}$ and $\bar{n}$ consistent with the measured ratio of $\Delta N_{\rm BG}/A$ of only $\sim 4\%$. Additional sources of error in the inferred phonon number, $\bar{n}^{\rm inf}$, are considered below.

FABRICATION

The nanobeam cavities were fabricated using a Silicon-On-Insulator wafer from SOITEC (ρ = 4-20 Ω·cm, device layer thickness t = 220 nm, buried-oxide layer thickness 2 μm). The cavity geometry is defined by electron beam lithography followed by inductively-coupled-plasma reactive ion etching (ICP-RIE) to transfer the pattern through the 220 nm silicon device layer. The cavities were then undercut using a HF:H_2O solution to remove the buried oxide layer, and cleaned using a piranha/HF cycle [7]. The dimensions and design of the nanobeam will be discussed in detail elsewhere.

DEVICE PARAMETERS

Under vacuum and cryogenic parameters, the optical resonance was found to have $Q_o = 4 \times 10^5$, $\omega_o/2\pi = 195$ THz ($\lambda = 1,537$ nm), and resonant transmission contrast of 25%. This corresponds to $\kappa/2\pi = 488$ MHz and $\kappa_e/2\pi = 65$ MHz. The mechanical mode was found to have $Q_m = 1.06 \times 10^5$ and $\omega_m/2\pi = 3.68$ GHz. This corresponds to $\gamma_i/2\pi = 35$ kHz. The optomechanical coupling rate was found to be $g/2\pi = 910$ kHz.

EXPERIMENTAL SETUP

The detailed experimental setup used to measure the cooling spectra and the electromagnetically-induced transparency (EIT) window of the optomechanical crystal is shown in Figure (S2). The setup is designed to measure both the EIT-like reflected signal and the transmission signal of the laser used to cool the mechanical system (though not simultaneously).

As a light source we use a fiber-coupled, tunable, near-infrared laser, (New Focus Velocity, model TLB-6328) spanning approximately 60 nm centered around 1,550 nm, which has its intensity controlled by a variable optical attenuator (VOA). A small percentage (10%) of the laser intensity is sent to wavemeter (WM, High Finesse, WS/6 High Precision) for passive frequency stabilization of the laser. To minimize polarization dependent losses on the electro-optical-modulator (EOM), a fiber polarization controller (FPC) is placed before it.

The EOM is driven by the microwave source (RF S.G., Agilent, model E8257D-520). The RF signal is composed of an amplitude modulated RF-signal carrier swept between $\Delta = 1 - 8$ GHz modulated at the lock-in detection frequency, $\omega_{\rm LI}$. As a result, the EOM modulation produces two probe sidebands at $\pm\Delta$, each with a small amplitude modulation at the lock-in frequency.

A small portion of the signal from the EOM output (10%) is used as a DC control signal to keep the EOM level locked, compensating for any low frequency power drift during the experiment. The remaining laser light is passed through a circulator, a 2×2 switch (SW1) (used to control the direction of the laser light through the Taper region), and a fiber polarization controller (FPC). It is then coupled to a tapered and dimpled optical fiber (Taper) which has its position controlled with nanometer-scale precision.

Switches 2 and 3 (SW2 and SW3) determine the path that the light transmitted through the taper follows. In the normal configuration (denoted by the solid blue path in Figure (S2)), the transmitted light is optically amplified by an erbium-doped fiber amplifier (EDFA) and then detected by a high-speed photoreceiver (D2, New Focus, model 1554-B) which is connected to a real-time spectrum Analyzer (RSA, Tektronix RSA3408B). Detector 3 (D3) is used to measured the DC transmission response of the cavity. Additionally, the transmitted power is measured via a power

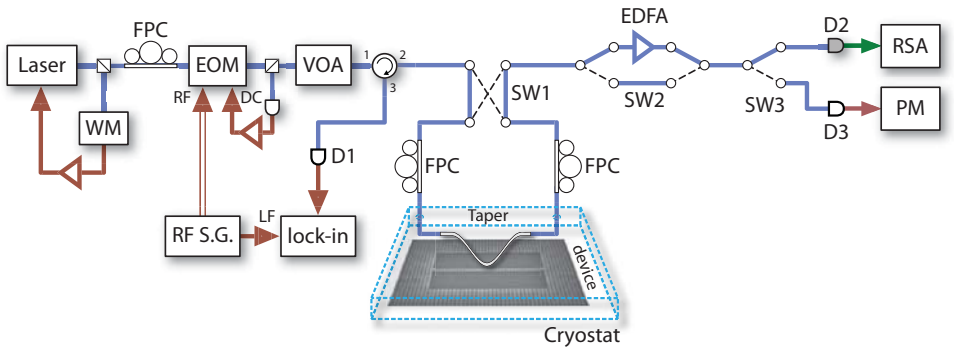

FIG. S2: **Detailed experimental setup.** Expanded experimental setup to include optical switches SW1, SW2 and SW3. The blue lines indicate the optical path for the cooling measurement (the '0' position of each of the switches), while the dashed black lines indicate the alternative switched paths (the '1' position of each of the switches). A single tunable laser is used as the cooling laser and mechanical transduction laser. A wavemeter (WM) is used to track and lock the laser's frequency to an absolute and relative value better than 100 MHz and 5 MHz, respectively. A calibrated (to better than 0.01 dB) variable optical attenuator (VOA) is used to set the cooling laser power. The transmitted component of the cooling laser beam that is sent into the optomechanical cavity is directed to an erbium-doped fiber amplifier (EDFA), where the optical signal is pre-amplified before being detected on a high-speed photodetector (D2). The measured photocurrent from D2 is sent to a real-time spectrum analyzer, where the mechanical noise power spectrum is measured. A slowly modulated optical signal, on-resonance with the optical nanobeam cavity, is generated from the cooling laser beam via an amplitude electro-optic modulator (EOM) driven by a microwave source (RFSG). The reflected component of the on-resonance laser signal injected into the cavity is separated from the input via an optical circulator, sent to a photodetector (D1), and then demodulated on a lock-in amplifier. Paddle-wheel fiber polarization controllers (FPCs) are used to set the laser polarization at the input to the EOM and the input to the optomechanical cavity.

meter (PM, Newport, model 2931-C). All the other configurations are used to calibrate the system as discussed in the calibration section.

Any reflected signal coming from the taper/device is detected by a high-gain photodetector (D1, New Focus, model 1811) and its signal is sent to a lock-in amplifier (L.I., SRS-830). The output from the in-phase and quadrature signals from the L.I. are recorded, producing the reflection scan shown in Figure (3c) of the main text.

EIT MEASUREMENTS

Here we will show how the amplitude modulation of the signal sideband Δ is used to measure the reflection ($|r(\omega)|^2$) of the signal reflected from the cavity. The output of the EOM can be written as

$$a_{\rm out}(t) = a_{\rm in}\Big[1+\beta\Big(1+m_{\rm LI}\cos(\omega_{\rm LI}t)\Big)\cos(\Delta t)\Big], \tag{S35}$$

where the input field amplitude $a_{\rm in}(t) = a_0 e^{i\omega_{\rm l}t}$, $a_0 = \sqrt{P_{\rm in}/\hbar\omega_{\rm l}}$, β is the EOM-modulation index, $\omega_{\rm LI}$ and $m_{\rm LI}$ are, respectively, the frequency and amplitude modulation index on the RF signal at Δ. For the measurements shown in the main text $m_{\rm LI} = 1$. In this case one can write the field of the EOM output (cavity input) in the time domain as

$$\begin{aligned} a_{\rm out}(t) = a_0\Bigg[&\cos(\omega_{\rm l}t) + \frac{\beta}{2}\Big[\cos((\omega_{\rm l}+\Delta)t) + \cos((\omega_{\rm l}-\Delta)t)\Big] + \dots \\ &\frac{\beta}{4}\Big[\cos((\omega_{\rm l}+\Delta+\omega_{\rm LI})t) + \cos((\omega_{\rm l}+\Delta-\omega_{\rm LI})t) + \dots \\ &\cos((\omega_{\rm l}-\Delta+\omega_{\rm LI})t) + \cos((\omega_{\rm l}-\Delta-\omega_{\rm LI})t)\Big]\Bigg]. \end{aligned} \tag{S36}$$

The reflected signal is filtered by the cavity dispersion and considering the case where the pump is on the red-side of the cavity ($\omega_{\rm l} < \omega_o$) the reflected field is

$$a_R(t) = r(\omega_s)\frac{a_0\beta}{4}\Big[\cos((\omega_{\rm l}+\Delta)t) + \cos((\omega_{\rm l}+\Delta)t + (\omega_{\rm LI}t-\varphi)) + \cos((\omega_{\rm l}+\Delta)t - (\omega_{\rm LI}t-\varphi))\Big]. \tag{S37}$$

First we assume that $r(\omega_s)$ is roughly constant over a range of $\omega_{\rm LI}$ which is true for $\omega_{\rm LI} < (\gamma_i + \gamma_{\rm OM})/2$. This implies that the smallest transparency window we could measure is on the order of the lock-in detection frequency. This limit on the transparency window size is reflected in Figure (4a) in the main text, where only transparency windows larger 200 kHz are reported.

We can now write the time average detected power spectral density on the photoreceiver (D1 in Figure (S2)) by taking the absolute square value of the reflected field and keeping only the terms with frequency smaller than the detector bandwidth. In this case

$$P|_{\omega_s} = \frac{a_o^2 \beta^2 R_{\rm PD} G_{\rm PD}}{8 R_L} |r(\omega_s)|^2 \left[3 + 4\cos(\omega_{\rm LI} t - \varphi) + \frac{1}{2}\cos(2\omega_{\rm LI} t - 2\varphi) + \mathcal{O}(2\omega_{\rm l}) \right], \tag{S38}$$

where $R_{\rm PD} = 1$ A/W is the detector responsivity, $G_{\rm PD} = 40,000$ V/A is the detector gain and $R_L = 50\ \Omega$ is the load resistance.

This signal is then sent to the lock-in which can measure independently the in-phase (X) and quadrature (Y) power spectral densities at $\omega_{\rm LI}$:

$$X|_{\omega_{\rm LI}} = \frac{a_o^2 \beta^2 R_{\rm PD} G_{\rm PD}}{4 R_L} |r(\omega_s)|^2 \cos(\varphi), \tag{S39}$$

$$Y|_{\omega_{\rm LI}} = \frac{a_o^2 \beta^2 R_{\rm PD} G_{\rm PD}}{4 R_L} |r(\omega_s)|^2 \sin(\varphi). \tag{S40}$$

It is then easy to see the reflection amplitude and phase are given by

$$|r(\omega_s)|^2 = \frac{4 R_L}{a_o^2 \beta^2 R_{\rm PD} G_{\rm PD}} \sqrt{X|^2_{\omega_{\rm LI}} + Y|^2_{\omega_{\rm LI}}}, \tag{S41}$$

$$\tan(\varphi) = \frac{Y|_{\omega_{\rm LI}}}{X|_{\omega_{\rm LI}}}. \tag{S42}$$

From the imparted change in the phase the signal delay is then calculated as:

$$\tau^{(\rm R)} = \frac{\varphi}{\omega_{\rm LI}}, \tag{S43}$$

where $\tau^{(\rm R)} > 0$ ($\tau^{(\rm R)} < 0$) represent a delay (advance) on the signal.

Here we have neglected the gain provided by the lock-in, which is important to determine the absolute value of $r(\omega_s)$. To account for that we calibrate the X channel by a normalized transmission curve taken with low input power. Our assumption is that the cavity-taper coupling is not affected by the input power. A analogous result can be found for the case where the control laser is on the blue side of the cavity ($\omega_{\rm l} > \omega_o$). A more detailed description of the EIT experiment can be found in [8].

ANALYZING THE MECHANICAL MODE SPECTRA

To determine the total spectral power at ω_m for a given measured spectra, we first subtract a background taken with the cooling laser far-detuned from the cavity (in the same calibration conditions). We then perform a least squares fit to a Lorentzian function of the form

$$L(\omega) = \frac{A}{\left(\frac{\omega - \omega_m}{2\gamma}\right)^2 + 1} \tag{S44}$$

with fit parameters A, ω_m and γ. The spectral power is then given simply by

$$P_{\omega_m} = \frac{A\gamma}{4}. \tag{S45}$$

To extract the intrinsic linewidth γ_i we first fix the input power $P_{\rm in}$. We then lock the pump on the red side of the cavity (at $\Delta = +\omega_m$) and measure the total linewidth, $\gamma_{\rm red} = \gamma_i + \gamma_{\rm OM}^{(\rm red)}$. We repeat the measurement on the blue side (at $\Delta = -\omega_m$), where $\gamma_{\rm blue} = \gamma_i - \gamma_{\rm OM}^{(\rm blue)}$. Using low input powers where $\gamma_{\rm OM}^{(\rm blue)} \ll \gamma_i$ to avoid amplification of the mechanical oscillations, we have $\gamma_{\rm OM}^{(\rm red)} = \gamma_{\rm OM}^{(\rm blue)}$, which leads to

$$\gamma_i = \frac{\gamma_{\rm red} + \gamma_{\rm blue}}{2}. \tag{S46}$$

MECHANICAL MODE THERMOMETRY

Equation (S11) shows an explicit form for the sideband power amplitude seen by a photodetector for a red detuned pump laser. More specifically we can find a relation between the number of phonons inside the cavity and the measured power spectrum for our experimental setup. As shown before, the RF-spectra are detected via a RSA which displays the power spectral density of the optical signal at D2 (with electronic gain G_e from the detector and optical gain $G_{\rm EDFA}$ from the EDFA). The single sided power spectral density at the detector is given by Equation (S11), and denoted $S_{\rm PP}(\omega)$. Since the power is related to voltage by an electronic gain G_e, then $S_{VV}(\omega) = G_e^2 S_{\rm PP}(\omega)$. When the EDFA is used, there is an additional gain factor, and $S_{VV}(\omega) = G_{\rm EDFA}^2 G_e^2 S_{\rm PP}(\omega)$. Finally, the RSA reports power as opposed to squared voltages, and so the final spectral density measured is $S(\omega) = S_{VV}(\omega)/2R_L$, where $R_L = 50\ \Omega$ is the input impedance of the RSA and the factor of two in the denominator comes from the conversion of peak-to-peak voltage to RMS voltage. Then, in terms of integrated power, the power detected in the sideband on the RSA, P_{ω_m}, is related to the heterodyne detected integrated spectral density by the relation

$$P_{\omega_m} = \frac{(G_e G_{\rm EDFA})^2}{2R_L} P_{\rm SB}, \tag{S47}$$

where Equations (S25) and (S8) have been used to rewrite the integrated form of Equation (S11) as

$$P_{\rm SB} = (\hbar\omega_0)^2 \frac{(\kappa_e/2) N_{\rm in}}{(\Delta - \omega_m)^2 + (\kappa/2)^2}\ \kappa(\gamma - \gamma_i)\bar{n}. \tag{S48}$$

From Equation (S47) we can write the expression that relates the number of phonons, $\bar{n}$, and all the system parameters as

$$\bar{n} = \left(\frac{2R_L}{G_e^2 G_{\rm EDFA}^2} \frac{P_{\omega_m}}{\hbar\omega_0}\right)\left(\frac{1}{\kappa(\gamma - \gamma_i)}\right)\left(\frac{(\Delta - \omega_m)^2 + (\kappa/2)^2}{(\kappa_e/2) P_{\rm in}}\right). \tag{S49}$$

Using Equation (S24), $\bar{n}$ can also be related to the bath temperature, T_b. To check the validity of this analysis, repeated measurements at room temperature were performed, yielding a T_b of $\sim 296 \pm 8$ K.

Measuring Device Parameters

From the DC transmission spectra, the optical components κ, κ_e and ω_0 can be determined. From the RF-spectra one can determine the intrinsic mechanical linewidth γ_i, the total mechanical linewidth $\gamma = \gamma_i + \gamma_{\rm OM}$, the mechanical frequency ω_m, and P_{ω_m}. The EIT spectra give the true detuning Δ between the pump laser and the cavity and provides an independent measure of $\gamma_{\rm OM}$ [8].

Calibration of Input Power

While the input/output optical power of the taper can be measured directly, the input power, $P_{\rm in}$, is additionally influenced by asymmetric losses in the taper resulting from coupling geometry. With this in mind, the 2×2 switch SW1 allows these losses to be characterized by switching the direction of the light through the taper. Labeling the two positions of the switch '0' and '1', the input powers at SW1, P_0 and P_1, and total insertion loss, $L_{\rm taper}$, are measured directly. Optical transmission scans are then taken in both switch positions at high enough powers to induce optical bistability. Given that the bistability shift of the optical mode, $\Delta\lambda_0$ and $\Delta\lambda_1$ for the two directions respectively, is proportional to the dropped power, we have

$$\frac{P_0 L_0}{P_1 L_1} = \frac{P_{\rm in,0}}{P_{\rm in,1}} = \frac{\Delta\lambda_0}{\Delta\lambda_1}, \tag{S50}$$

where L_0 and L_1 are the losses before the cavity, and $P_{\rm in,0}$ and $P_{\rm in,1}$ are the powers at the cavity, in the respective switch positions. Since $L_0 L_1 = L_{\rm taper}$, $P_{\rm in}$ for both switch positions can be determined (though during the measurement, the direction of the light through the taper is fixed).

Calibration of EDFA Gain

The EDFA gain, $G_{\rm EDFA}$, is measured by utilizing SW2 to insert and remove the EDFA from the optical train, while measuring a fixed tone at the mechanical frequency, ω_m, generated by the EOM. The ratio of the integrated spectral power of the tones gives $G^2_{\rm EDFA}$.

Calibration of Electronic Gain

To characterize the electronic gain, G_e, of detector D2, we first maximize the power incident on the detector (by reducing the attenuation on the VOA). We then measure the DC bias voltage $V_{\rm DC,0}$ (via the bias monitor port on D2) and verified that this voltage was identical to the DC voltage at the high frequency port on D2, ensuring that $V_{\rm DC,0}$ accurately reflected the voltage measured by the RSA. Then, using switch SW3, the power incident on D3, $P_{\rm D3,0}$, was also measured. For each data point in the experiment (corresponding to a different attenuation), we measure the incident power on D3, $P_{\rm D3}$. We have then

$$V_{\rm DC} = V_{\rm DC,0}\frac{P_{\rm D3}}{P_{\rm D3,0}}. \tag{S51}$$

The purpose of this is a technical one; the dynamic range of our optical power meter is much larger than that of our voltmeter, allowing the DC bias voltage of the detector to be determined for any amplitude of optical signal. Since Equation (S48) is computed at the cavity, the electronic gain must reflect the conversion of power at the cavity, $P_{\rm in}$, to voltage at the detector, $V_{\rm DC}$, giving $G_e = V_{\rm DC}/P_{\rm in}$ (for $V_{\rm DC}$ and $P_{\rm in}$ measured at the same attenuation). We note that this is not the gain typically quoted on a specification sheet; it encapsulates the optical insertion loss between the cavity and the detector in our experimental setup.

Error Analysis

We can calculate the cumulative error for the measured intracavity phonon number using Equation (S49) and statistics on the set of measurable parameters, giving

$$\frac{\Delta\bar{n}}{\bar{n}} = \Bigg[\frac{\delta\omega_0^2}{\omega_0^2} + \frac{\delta\kappa_e^2}{\kappa_e^2} + \frac{\delta P_{\rm in}^2}{P_{\rm in}^2} + \frac{\delta P_{\rm D3}^2}{P_{\rm D3}^2} + \frac{\delta\gamma_i^2}{(\gamma-\gamma_i)^2} + \frac{\delta\gamma^2}{\gamma-\gamma_i)^2} + \dots \tag{S52}$$
$$\left(\frac{\kappa/2}{(\kappa/2)^2+(\Delta-\omega_m)^2} - \frac{1}{\kappa}\right)^2\delta\kappa^2 + \left(\frac{2(\Delta-\omega_m)}{(\kappa/2)^2+(\Delta-\omega_m)^2}\right)^2\delta\Delta^2 + \left(\frac{2(\Delta-\omega_m)}{(\kappa/2)^2+(\Delta-\omega_m)^2}\right)^2\delta\omega_m^2\Bigg]^{1/2}.$$

Here we neglected the error on G_e and $G_{\rm EDFA}$ which are much smaller than any other error quantity. To determine the variation for κ, κ_e and ω_0, we measured the DC optical spectrum for every single data point in Figure (4b) of the main text and determined $\delta\kappa$, $\delta\kappa_e$ and $\delta\omega_0$ from the normalized standard deviations of each of the values. The measurement uncertainty of these values are below 0.7%. The mechanical properties $\delta\gamma$, $\delta P_{\rm D3}$ and $\delta\omega_m$, were determined from the deviation on the spectra fits using a 95% confidence interval, which produces percent errors below 0.6%. The pump laser detuning from the cavity is controlled by the EIT reflection spectra. To find the variation of the detuning $\delta\Delta$ we once again computed the standard deviation of all the measured detunings, which results in a deviation of less than 0.3%.

Finally, the two main sources of error in our data are the determination of the intrinsic mechanical quality factor (reflected in γ_i) and the input power, $P_{\rm in}$. The uncertainty in the mechanical linewidth, $\delta\gamma_i$, is found by repeatedly measuring it at a single power level and computing its standard deviation (found to be $\sim 1.6\%$). Using the calibration procedure discussed above for $P_{\rm in}$, the error lies in the determination of losses L_0 and L_1. In the worst case the calibration would be off by the ratio between the input loss, L_0 in the present experiment, and the square root of total loss $\sqrt{L_0L_1}$ producing a percentage error of $\sim 4.0\%$ to the input power.

Taking all of these factors into account, as well as the optical noise discussed above, we find an overall uncertainty of $\sim 9\%$ in the measured absolute phonon number at the maximum cooling point.

ESTIMATING THE TEMPERATURE SHIFT FROM THERMO-OPTIC EFFECTS

Absorption in the dielectric cavity causes the temperature of the dielectric cavity to increase locally. This effect is expressed through shifts in the refractive index of the structure, and the thermo-optic coefficient of Silicon [9]. As such, we can estimate the temperature of the cavity by looking at the shift in the cavity frequency, starting from a known temperature.

The starting point of the analysis is the cavity-perturbation formula for dielectric cavities [10],

$$\frac{\omega - \omega_0}{\omega_0} \approx -\frac{1}{2}\frac{\int \delta\epsilon(\mathbf{r})|\mathbf{E}(\mathbf{r})|^2 \mathrm{d}\mathbf{r}}{\int \epsilon(\mathbf{r})|\mathbf{E}(\mathbf{r})|^2 \mathrm{d}\mathbf{r}}. \tag{S53}$$

From the relation $\epsilon/\epsilon_0 = n^2$, we find $\delta\epsilon = 2n\delta n\epsilon_0$. By assuming that the cavity as a whole is heated to a temperature T_0, the integral in Equation (S53) can be written as

$$\omega - \omega_0 \approx -n(T_0)\omega_0 \frac{\int_{\mathrm{Si}} |\mathbf{E}(\mathbf{r})|^2 \mathrm{d}\mathbf{r}}{\int (n(T_0))^2 |\mathbf{E}(\mathbf{r})|^2 \mathrm{d}\mathbf{r}} \times (n(T) - n(T_0)). \tag{S54}$$

Using the values of $n(T)$ found in literature [9], and a value of

$$\frac{\int_{\mathrm{Si}} |\mathbf{E}(\mathbf{r})|^2 \mathrm{d}\mathbf{r}}{\int (n(T_0))^2 |\mathbf{E}(\mathbf{r})|^2 \mathrm{d}\mathbf{r}} \approx 7.5066 \times 10^{-2},$$

calculated from the finite element simulations (FEM) of the mode profiles, we plot the wavelength shift from 17.6 K up to 300 K in Figure (S3a). The total shift of 12.0 nm agrees with the experimentally observed change in resonance wavelength.

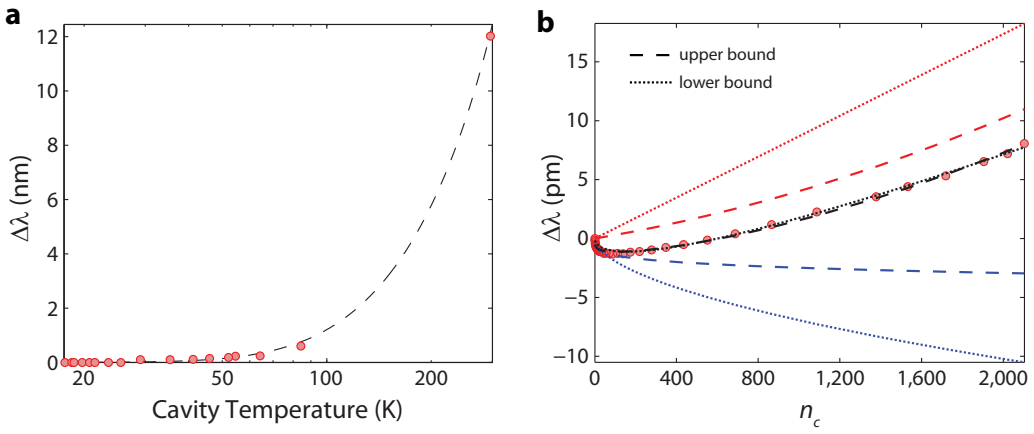

FIG. S3: **Thermo-optic effects. a**, The measured wavelength shift compared to the theoretical shift predicted by Equation (S54) for a range of cavity temperatures, using 17.6 K as the reference point. **b**, The measured power-dependent wavelength shift of the cavity with fitted individual contributions due to free carrier dispersion (blue) and refractive index change (red), as well as their sum (black), for the two bounds discussed in the text.

This analysis can be applied to the wavelength shift data for various input powers at low temperature where the initial cavity temperature is measured by thermometry methods discussed above. We note an initial blue-shift of the cavity, which is attributed to free-carrier dispersion effects [11] and can be modeled by a power law dependence on intracavity photon number, $A(n_c)^B$. The temperature-dependent data for the refractive index of Silicon in [9] is valid only for $T > 30$ K so the power-dependent cavity heating for a starting temperature of 17.6 K, for the largest intracavity photon number, can only be bounded. For the upper bound, we assume $dn/dT = 0$ for $T < 30$ K, resulting in a ΔT_{max} of 16.8 K. For the lower bound, we assume $dn/dT = dn/dT|_{T=30\ \mathrm{K}}$ for $T < 30$ K, resulting in a ΔT_{min} of 7.8 K. These bounds and their respective fits are shown in Figure (S3b).

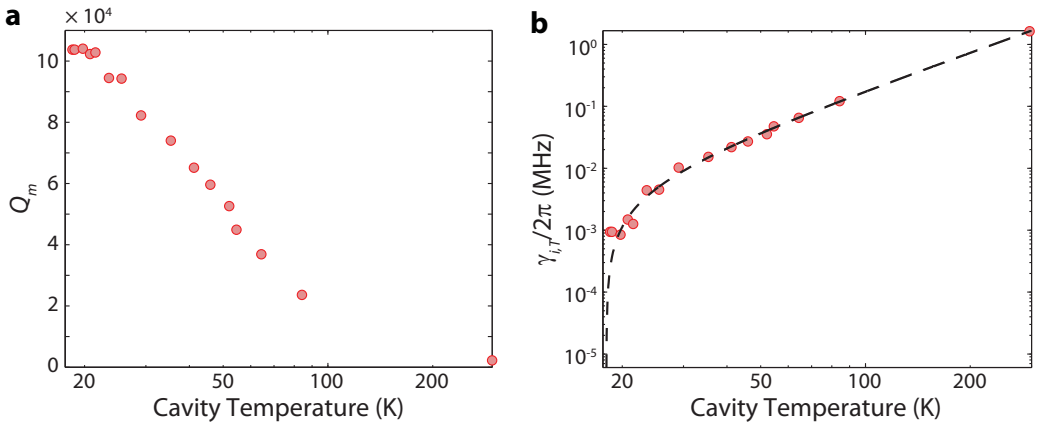

FIG. S4: **Temperature dependent loss. a**, The measured intrinsic mechanical quality factor for various cavity temperatures. **b**, The inferred intrinsic mechanical loss rate due to temperature, $\gamma_{i,T}$, modeled by a 4th order polynomial fit.

TEMPERATURE-DEPENDENT MODIFICATIONS TO THE INTRINSIC MECHANICAL DAMPING

Independent measurements of the mechanical quality factor, Q_m, at varying bath temperatures indicate that the Q_m changes with temperature (Figure (S4a)). These measurements are taken at low intracavity photon number, rendering free-carrier effects negligible. As such we can model the mechanical loss rate as $\gamma_i(T) = \gamma_{i,T}(T) + \gamma_i^{(0)}$ where $\gamma_i^{(0)}$ is the measured loss rate at the reference temperature (17.6 K). The extracted form of $\gamma_{i,T}(T)$ is shown in Figure (S4b). However, the mechanism governing this temperature dependent loss is currently unknown, and is the topic of future studies.

PHOTON-NUMBER DEPENDENT MODIFICATIONS TO THE INTRINSIC MECHANICAL DAMPING

The deviation of the expected cooled phonon number from the measured value is a result of two factors: bath heating and an increase in the intrinsic mechanical loss rate (γ_i) due to heating and free carriers. Since the integrated spectral power of the mechanical mode depends only on the product $\gamma_i T_b$ (for large intracavity photon numbers n_c), naively ignoring the latter effect results in an estimated change of $\Delta T > 50$ K in the bath temperature for 2,000 intracavity photons. This is unrealistic as such a temperature change would tune the optical mode red by > 300 pm (from Equation (S54)), while the actual measured shift is closer to $10 - 20$ pm (from Figure (S3b)). In fact through independent measurements (where dynamic back-action was minimized), we found that the mechanical linewidth is a function of the number of photons in the cavity. We attribute this to a nonlinear process in the cavity involving the generation of free carriers, which will be explored in depth elsewhere, and introduce an additional loss channel $\gamma_{i,\mathrm{FC}}$ in the mechanical loss rate so that we have

$$\gamma_i \to \gamma_i \equiv \gamma_i^{(0)} + \gamma_{i,T}(T(n_c)) + \gamma_{i,\mathrm{FC}}(n_c). \tag{S55}$$

From the relations shown on previous sections, we have $\gamma_{\mathrm{cooled}}^{(0)} = \gamma_i^{(0)} + \gamma_{\mathrm{OM}}$. Incorporating Equation (S55), we have experimentally, $\gamma_{\mathrm{cooled}} = \gamma_i + \gamma_{\mathrm{OM}}$, with their difference yielding the magnitude of the additional loss rates. However, for $\Delta = \omega_m$ and $n_c > 10$, γ_{OM} tends to be large compared to γ_i, making this subtraction quite error prone. Thus, to get accurate data for high intracavity photon numbers we use a range of larger detunings, noting that $\gamma_{\mathrm{OM}} \propto \Delta^{-2}$ for $\Delta \gg \omega_m$ and fixed n_c (approximately). This loss is then modeled using a power law dependence on n_c (Figure (S5a)).

Using the models of mechanical loss from Figure (S5a) and Figure (S4b) with the thermometry technique outlined earlier (making the replacement to γ_i) allows a more accurate determination of the temperature rise in the cavity, as well as the characterization of the individual contributions of $\gamma_{i,T}$ and $\gamma_{i,\mathrm{FC}}$ as a function of n_c. The result is an estimated increase of 13.2 K in T_b at the highest input power, well within the previously fitted temperature bounds.

The addition of a free carrier related loss channel is further corroborated by pumping the Si sample above the band gap with a 532 nm solid state green laser, directly stimulating the production of free carriers. The degradation in Q_m can be only partially explained by heating due to absorption since the maximum 19 K temperature rise estimated

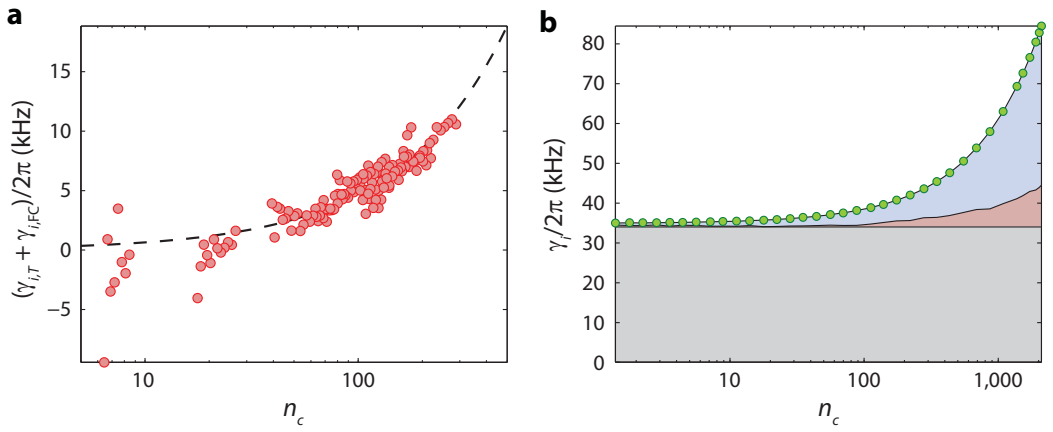

FIG. S5: **Photon number dependent loss. a**, Excess loss as a function of n_c, inferred from far-red-detuned ($\Delta > 5.5$ GHz) measurements of $\gamma_{\rm cooled}$. **b**, Breakdown showing the individual contributions of $\gamma_i^{(0)}$ (gray), $\gamma_{i,T}$ (red), and $\gamma_{i,\rm FC}$ (blue) to the total γ_i (○).

from the cavity red-shift results in an expected Q_m of approximately 70,000 at the highest power (Figure (S4a)), whereas a far lower value is measured. The remaining excess loss is attributed to the presence of free-carriers. These results are shown in Figure (S6).

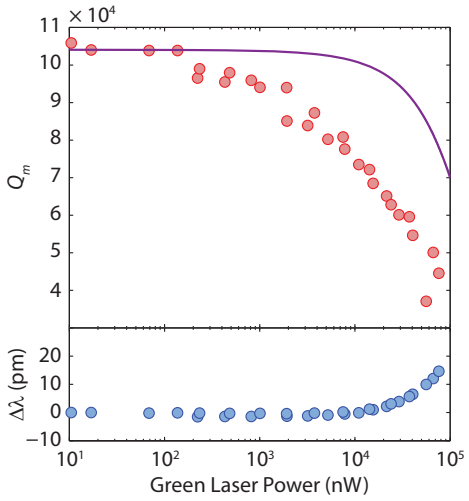

FIG. S6: **Loss due to free-carriers.** The Q_m degradation as a function of 532 nm laser power. The purple line shows the expected Q_m for the bath temperature rise inferred from the wavelength shift data. The deviation of the data from this prediction suggests an additional loss channel related to the presence of free carriers.

AMPLIFIER NOISE CONSIDERATIONS

We consider here the impact of using a non-ideal amplifier (EDFA) on the measured signal, and the deviation from quantum limits of motion transduction. For a coherent optical beam with frequency $\omega_{\rm l}$ and power P incident on a photodetector, the single sided power spectral density of the optical shot noise is simply

$$S_{\rm shot}(\omega) = \sqrt{2\hbar\omega_{\rm l} P}, \tag{S56}$$

independent of frequency. If we consider the EDFA gain, $G_{\rm EDFA}$, and the optical insertion loss between the output of the cavity and the input of the EDFA, $1-\eta_d$ (measured to be 2.2 dB), the corresponding noise at the output of

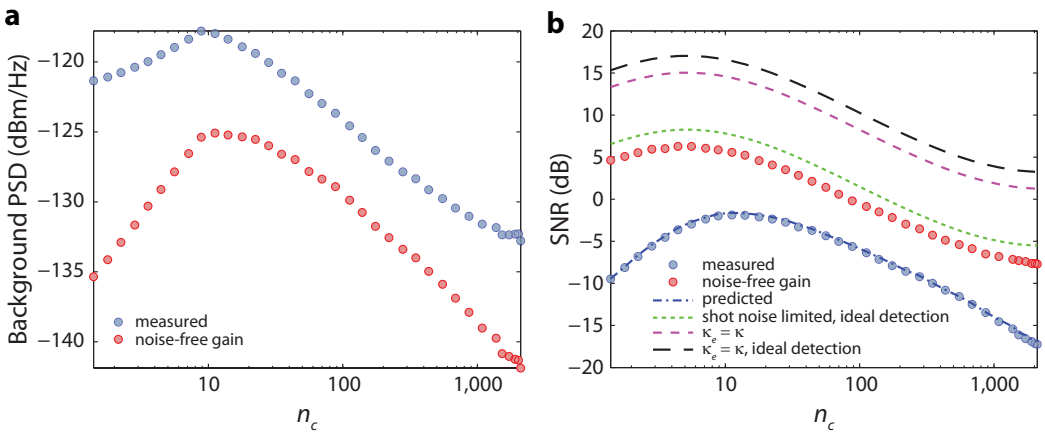

FIG. S7: **Effect of amplifier noise and optical losses on the measured signal.** **a**, Comparison of the measured background NPSD to the shot noise level of the cooling laser beam amplified by an ideal, noise-free amplifier. **b**, Comparison of the SNR for several different cases. (i) Experimental device and measurement conditions of this work. Measured (blue ∘) and predicted SNR (blue dot-dashed curve) are both shown. (ii) Shot-noise-limited SNR with noise-free amplification and unit-quantum-efficiency photodetection, all other device parameters as in the experiment. SNR shown with (red ∘) and without (dashed green curve) optical loss between the output of the cavity and the input to the optical amplifier. (iii) Noise-free amplification and unit-quantum-efficiency photodetection along with ideal coupling to the cavity system (i.e., single-sided coupling with no other optical loss channels, which in the notation described above yields, $\kappa = \kappa_e/2$). This is plotted with (purple dashed curve) and without (black dashed curve) the optical insertion loss between the output of the cavity and photodetection. The dashed black curve thus represents an ideal quantum-limited transducer of mechanical motion.

the amplifier assuming noise-free amplification is given by

$$S_{\text{shot,amplified}} = G_{\text{EDFA}}\sqrt{2\hbar\omega_l\eta_d P_{\text{in}}}, \tag{S57}$$

where P_{in} is the optical power at the input of the cavity and $\eta_d P_{\text{in}}$ is the optical power reaching the input to the EDFA. We use the term "noise-free amplification" here to indicate an amplifier process in which the signal-to-noise ratio (SNR) at the output is equal to that at the input (i.e., an amplifier noise figure of 0 dB). Using the electronic gain, G_e, obtained from calibrations, the theoretical background noise power spectral density (NPSD) measured by the RSA, corresponding to noise-free amplification of shot noise on the optical cooling beam can be found. To wit,

$$S^2_{\text{shot,amplified,RSA}} = (S_{\text{shot,amplified}})^2 \left(\frac{G_e}{\eta_d}\right)^2 \frac{1}{R_L}, \tag{S58}$$

where R_L is the input impendence to the RSA and the ratio G_e/η_d is the electrical conversion factor for optical power at the output of the EDFA (η_d accounts for the loss between the cavity and the EDFA, while G_e accounts for the *total* insertion loss between the cavity and the detector). This is plotted against the measured background NPSD in Figure (S7a). The trend seen in Figure (S7a) versus cooling beam power (plotted in units of intracavity photon number, n_c) is a result of the varying EDFA drive current versus n_c used in our experiment. Specifically, for intracavity photon populations < 10, we are limited by the highest gain setting of the EDFA. In this regime, the EDFA drive current (and thus gain) remains constant, resulting in the increasing background NPSD with cooling beam optical power. For larger intracavity photon numbers, we are limited by the saturation power of the detector D2. In this regime, the EDFA drive current (gain) is reduced to avoid detector saturation, resulting in the decreasing background NPSD with optical cooling beam power. The difference between the noise-free gain background level modeled by Equation (S58) and the measured background level, reflects the added noise due to the EDFA (its noise figure). An ideal EDFA amplifier adds 3 dB of noise above the shot noise level [12]. In a real EDFA device, however, the noise figure of the amplifier depends on both the input power and EDFA drive current (amplifier inversion level). We define the added EDFA optical noise as the noise above that for a noise-free amplification process,

$$S_{\text{excess}} \equiv \sqrt{\frac{S^2_{\text{background}} - S^2_{\text{shot,amplified,RSA}}}{(G_e/\eta_d)^2\,(1/R_L)}}, \tag{S59}$$

where $S^2_{\text{background}}$ is the actual noise floor of the NPSD at the output of the EDFA. Although the EDFA adds excess noise, its utility stems from the fact that the gain provided by the EDFA overcomes the electronic noise in the photodetectors and RSA, non-unity quantum efficiency in the photodetectors, and optical insertion loss between the EDFA and detector D2, with a resulting overall SNR penalty of only $S^2_{\text{excess}}/\eta_d$ (derived below).

In addition to broadband noise, the optical cooling beam signal at the output of the cavity also contains information about the mechanical motion of the localized acoustic mode in the nanobeam cavity. As shown in Equation (S22), the transduced mechanical motion results in a narrow Lorentzian signal centered at the mechanical frequency that sits on top of the noise floor in the NPSD of the transmitted optical beam. Defining the SNR for this measurement as the ratio between the peak of the Lorentzian component to that of the background in the measured NPSD, we can determine how the different non-idealities of the measurement process (such as cavity coupling, optical loss, and amplifier excess noise) impact the sensitivity of our measurement of mechanical motion. For example, the theoretical shot-noise-limited SNR, corresponding to noise-free amplification, ideal photodetection, and no optical insertion loss after the cavity is given by,

$$\text{SNR}_{\text{shot}} = \frac{4P_{\text{SB}}/2(\gamma_i + \gamma_{\text{OM}})}{2\hbar\omega_o P_{\text{in}}}, \tag{S60}$$

where the numerator is the theoretical cooled peak signal amplitude due to mechanical motion given by Equation (S48) for a particular n_c (note that we include in this signal amplitude the effects of the power dependent bath temperature shift and modifications to the intrinsic mechanical damping rate γ_i, as discussed above). In Figure (S7b) we consider several cases for comparison:

i. Measurement and cavity parameters as used this work (all non-idealities included). The actually measured SNR along with a predicted SNR based upon independent measurement and calibration of the device and experimental setup are shown. For the predicted SNR we have,

$$\begin{aligned}\text{SNR}_{\text{predicted}} &= \frac{4G^2_{\text{EDFA}}G_e^2 P_{\text{SB}}/2R_L(\gamma_i + \gamma_{\text{OM}})}{S^2_{\text{background}}} \\ &= \frac{4G^2_{\text{EDFA}}P_{\text{SB}}/2(\gamma_i + \gamma_{\text{OM}})}{2\hbar\omega_o G^2_{\text{EDFA}}P_{\text{in}} + S^2_{\text{excess}}/\eta_d}\eta_d,\end{aligned} \tag{S61}$$

which closely corresponds to the actual measured SNR values, as seen in Figure (S7b). The deviation of the curve shape of the measured SNR from the other cases is attributed primarily to the variance in the excess noise added by the EDFA amplification.

ii. Shot-noise-limited detection, with and without loss in the optical path after the cavity (all other cavity parameters and non-idealities as per the measured device). In the case with optical loss in the optical path we have instead of Equation (S60),

$$\text{SNR}_{\text{shot,lossy}} = \frac{4P_{\text{SB}}/2(\gamma_i + \gamma_{\text{OM}})}{2\hbar\omega_o P_{\text{in}}}\eta_d, \tag{S62}$$

where $1 - \eta_d$ is the insertion loss discussed above.

iii. An ideally coupled cavity system with shot-noise-limited detection. In this case we consider a perfect single-sided cavity system in which $\kappa = \kappa_e/2$ with all other device parameters constant and non-idealities present (excluding added amplifier noise). We repeat the same analysis for the insertion-loss-free case, representing an optimal (quantum-limited) transduction of motion.

Considering all the above cases one can infer that a significant fraction of the degradation in our measured SNR from that of an ideal quantum-limited transducer stems from the non-ideality of our cavity loading (photons carrying information regarding the mechanical motion are lost into non-detected channels). The remaining inefficiencies in our detection process are a result of the added noise due to the non-ideality of the EDFA amplification and the small amount (~ 2 dB) of optical loss in the optical path between the cavity output and the EDFA.

MEASUREMENT IMPRECISION

In considering the limits of a continuous position measurement of the mechanical motion of an object one typically defines a measurement imprecision level related to the power spectrum noise floor on top of which the position signal

sits [13]. Conventionally, the imprecision level corresponding to the background NPSD in the power spectrum of the measured signal is expressed in terms of a mechanical displacement sensitivity with units of m^2/Hz. From the discussion above, the PSD of the measured output signal in our case (transmission of the optical cooling beam) is proportional to

$$S_{II}(\omega) = B + \frac{\kappa_e}{2\kappa}\frac{8|G|^2}{\kappa}\bar{S}_{bb}(\omega). \tag{S63}$$

The background NPSD is set by the constant B, which for unit quantum efficiency and shot-noise-limited photodetection, is unity (though for the current measurement, $B > 1$ due to added EDFA amplifier noise and optical loss). Since $\bar{S}_{bb}(\omega)$ is proportional to $\bar{n}$ (see Equation (S23)), it is natural to consider the imprecision level of our measurements (due to the background noise level) in units of phonon quanta. The background NPSD in units of "quanta" is simply

$$S^2_{\text{background}}\big|_{\text{quanta}} = \bar{n}\left(\frac{B}{\frac{\kappa_e}{2\kappa}\frac{8|G|^2}{\kappa}\bar{S}_{bb}(\omega=\omega_m)}\right). \tag{S64}$$

A background NPSD, or imprecision level, of $n_{\text{imp}} = 1$ then, corresponds to the equivalent level of NPSD in the output signal that would be produced at the peak of the Lorentzian signal by a single quanta in the mechanical oscillator. For the case of noise-free optical amplification, unit-quantum-efficiency photodetection, and ideal coupling ($\kappa = \kappa_e/2$), the value of the constant B is unity and the background NPSD approaches 1/4 quanta in the large cooperativity limit.

One can convert between an imprecision level in units of quanta and the more conventional m^2/Hz through the relation

$$S^2_{\text{background}}\big|_{m^2/Hz} = \left(\frac{4}{\gamma}\right)\left(2x^2_{\text{zpf}}\right) S^2_{\text{background}}\big|_{\text{quanta}}, \tag{S65}$$

where one phonon quanta has $2x^2_{\text{zpf}}$ worth of displacement noise power which is dispersed over a bandwidth γ (the peak NPSD is $4/\gamma$ times the total noise power). The standard quantum limit (SQL) of displacement sensitivity corresponding to an on-resonance (single-sided) NPSD is equal to $\text{SQL}_x(\omega=\omega_m) = \left(x^2_{\text{zpf}}/2\right)(4/\gamma)$, or one-quarter quanta's worth of displacement noise power. Therefore, in terms of this SQL displacement sensitivity, the imprecision levels are related as $S^2_{\text{background}}\big|_{m^2/Hz} = (4\text{SQL}_x)\, S^2_{\text{background}}\big|_{\text{quanta}}$. Note that the spectra of the measured NPSD in the insets of Figure (4b) of the main text are given in units m^2/Hz. In order to determine the zero-point-fluctuation amplitude, $x_{\text{zpf}} = \sqrt{\hbar/2m\omega_m}$ for these plots, we numerically compute the effective motional mass, m, as in Ref. [1]. FEM simulations of the mechanical breathing mode of the nanobeam cavity yields a motional mass of $m = 311$ fg and a corresponding zero-point-fluctuation amplitude of $x_{\text{zpf}} = 2.7$ fm.

---

† Present address: Instituto de Física "Gleb Wataghin", Universidade Estadual de Campinas, UNICAMP, 13083-859, Campinas, SP, Brazil

* Electronic address: opainter@caltech.edu; URL: http://copilot.caltech.edu

[1] Eichenfield, M., Chan, J., Camacho, R. M., Vahala, K. J. & Painter, O. Optomechanical crystals. *Nature* **462**, 78–82 (2009).

[2] Wilson-Rae, I., Nooshi, N., Zwerger, W. & Kippenberg, T. J. Theory of ground state cooling of a mechanical oscillator using dynamical back-action. *Phys. Rev. Lett.* **99**, 093901 (2007).

[3] Marquardt, F., Chen, J. P., Clerk, A. A. & Girvin, S. M. Quantum theory of cavity-assisted sideband cooling of mechanical motion. *Phys. Rev. Lett.* **99**, 093902 (2007).

[4] Safavi-Naeini, A. H. & Painter, O. Proposal for an optomechanical traveling wave phonon-photon translator. *New J. Phys.* **13**, 013017 (2011).

[5] Rocheleau, T. *et al.* Preparation and detection of a mechanical resonator near the ground state of motion. *Nature* **463**, 72–75 (2010).

[6] Rivière, R. *et al.* Optomechanical sideband cooling of a micromechanical oscillator close to the quantum ground state. *Phys. Rev. A* **83**, 063835 (2011).

[7] Borselli, M., Johnson, T. J. & Painter, O. Measuring the role of surface chemistry in silicon microphotonics. *App. Phys. Lett.* **88**, 131114 (2006).

[8] Safavi-Naeini, A. H. *et al.* Electromagnetically induced transparency and slow light with optomechanics. *Nature* **472**, 69–73 (2011).

[9] Frey, B. J., Leviton, D. B. & Madison, T. J. Temperature-dependent refractive index of silicon and germanium. In *Proc. SPIE*, vol. 6273, 62732J (2006).
[10] Harrington, R. F. *Time-Harmonic Electromagnetic Fields* (IEEE Press, 1961).
[11] Barclay, P., Srinivasan, K. & Painter, O. Nonlinear response of silicon photonic crystal microresonators excited via an integrated waveguide and fiber taper. *Opt. Express* **13**, 801–820 (2005).
[12] Desurvire, E., Bayart, D., Desthieux, B. & Bigo, S. *Erbium-Doped Fiber Amplifiers, Device and System Developments* (Wiley-Interscience, 2002).
[13] Clerk, A. A., Devoret, M. H., Girvin, S. M., Marquardt, F. & Schoelkopf, R. J. Introduction to quantum noise, measurement, and amplification. *Rev. Mod. Phys.* **82**, 1155–1208 (2010).